Materials Today Bio 31 (2025) 101564

Contents lists available at ScienceDirect

Materials Today Bio

journal homepage: www.journals.elsevier.com/materials-today-bio

An aggregation-induced emission-active lysosome hijacker: Sabotaging lysosomes to boost photodynamic therapy efficacy and conquer tumor therapeutic resistance

Hang Zou [a,c,1], Pingping Wang [a,1], Zhihao Bai [a,1], Liping Liu [a], Jingtong Wang [a], Yanfang Cheng [a], Bairong He [a,c,d,***], Zujin Zhao [b,**], Lei Zheng [a,*]

[a] Department of Laboratory Medicine, Guangdong Provincial Key Laboratory of Precision Medical Diagnostics, Guangdong Engineering and Technology Research Center for Rapid Diagnostic Biosensors, Guangdong Provincial Key Laboratory of Single-cell and Extracellular Vesicles, Nanfang Hospital, Southern Medical University, Guangzhou, 510515, China

[b] State Key Laboratory of Luminescent Materials and Devices, Key Laboratory of Luminescence from Molecular Aggregates of Guangdong Province, South China University of Technology, Guangzhou, 510515, China

[c] De Feng Academy, Southern Medical University, Guangzhou, 510515, China

[d] Department of Medical Laboratory, Ganzhou Hospital-Nanfang Hospital, Southern Medical University, Ganzhou, 341000, China

ARTICLE INFO

Keywords:
Aggregation-induced emission
Therapeutic resistance
Photodynamic therapy
Therapeutic sensitizer
Lysosomal membrane permeabilization

ABSTRACT

Therapeutic resistance is a major challenge in clinical cancer theranostics, often leading to treatment failure and increased patient mortality. Breaking this therapeutic deadlock, enhancing the efficacy of clinical treatments, and ultimately improving patient survival rates are both highly desirable and significantly challenging goals. Herein, we have developed a new fluorescent luminogen, QM-DMAC, which features aggregation-induced emission (AIE), and exceptional viscosity-responsive properties. The AIE-active QM-DMAC can specifically stain lysosomes in tumor cells, offering a high signal-to-noise ratio and enabling specific visualization of variations in lysosomal viscosity, such as those induced by inflammation or autophagy. Furthermore, QM-DMAC effectively generates reactive oxygen species (ROS) under white light irradiation, which precisely induces ROS-mediated lysosomal membrane permeabilization (LMP) and lysosome rupture. This ultimately causes severe cell damage and restores the sensitivity of tumor cells to radiotherapy and chemotherapy. Thus, QM-DMAC serves as a highly efficient lysosome-targeting photosensitizer and an excellent therapeutic sensitizer. This innovative "lysosome hijacking" strategy significantly maximizes the efficacy of photodynamic therapy, conquering therapeutic resistance and boosting the synergistic therapeutic effect when integrated with conventional radiotherapy or chemotherapy. It provides a novel approach to the design of theranostic agents for clinical cancer theranostics.

1. Introduction

Despite the significant strides in tumor prevention and theranostics, cancer remains a disease with high mortality rates and presents substantial global challenges. In particular, therapeutic resistance is one of the primary reasons for poor patient outcomes, leading to suboptimal treatment responses, metastasis, and tumor recurrence, ultimately leads to therapeutic failure and increased patient mortality [1,2]. In clinical practice, therapeutic resistance impacts a wide range of tumors and is associated with virtually all anticancer treatments, including

* Corresponding author.

** Corresponding author. State Key Laboratory of Luminescent Materials and Devices, Key Laboratory of Luminescence from Molecular Aggregates of Guangdong Province, South China University of Technology, Guangzhou, 510640, China.

*** Corresponding author. Department of Laboratory Medicine, Guangdong Provincial Key Laboratory of Precision Medical Diagnostics, Guangdong Engineering and Technology Research Center for Rapid Diagnostic Biosensors, Guangdong Provincial Key Laboratory of Single-cell and Extracellular Vesicles, Nanfang Hospital, Southern Medical University, Guangzhou, 510515, China.

E-mail addresses: nfyyhbr@smu.edu.cn (B. He), mszjzhao@scut.edu.cn (Z. Zhao), nfyyzhenglei@smu.edu.cn (L. Zheng).

[1] These authors contributed equally to this work.

https://doi.org/10.1016/j.mtbio.2025.101564
Received 15 December 2024; Received in revised form 22 January 2025; Accepted 7 February 2025
Available online 8 February 2025

radiotherapy and chemotherapy—conventionally the primary treatments for cancer [3]. Therapeutic resistance involves multiple mechanisms, which can be present from the outset, rendering tumors insensitive to ionizing radiation or specific antitumor drugs, or they may develop over the course of therapy. Such mechanisms are categorized into either intrinsic or acquired resistance [4]. Furthermore, during tumor initiation and development, the heterogeneity of tumors, characterized by a diversity of genetic and molecular phenotypes, poses another crucial challenge to therapeutic resistance. Otherwise, malignant tumors often exhibit simultaneous resistance to different treatments, significantly reducing the efficacy of clinical therapies and ultimately leading to increased mortality [5]. These complex mechanisms and causes of therapeutic resistance highlight the significant challenge of addressing this issue. However, all of the above situations also underscore the potential for developing antagonists to therapeutic resistance in cancer, which could represent a promising strategy for clinical therapy [6–8]. With these agents, it is possible to restore tumor cell sensitivity toward conventional treatments such as radiotherapy and chemotherapy, thereby enhancing their efficacy [9,10]. The strategy aimed at leveraging the benefits of combination therapy is a promising approach to breaking the therapeutic deadlock. Consequently, developing a therapeutic sensitizer that can integrate and adapt conventional treatments to overcome therapeutic resistance is an urgent and promising strategy for future cancer therapeutics.

Lysosomes, critical cellular organelles, perform key functions in secretion, degradation, and signal transduction. They regulate cell proliferation, differentiation, metabolism, and apoptosis. Serving as cellular shields, lysosomes protect cells from drugs, toxic materials and foreign substances [11,12]. In tumor cells, lysosomes have been found to undergo diverse changes that are linked to malignant transformation, encompassing variations in lysosome quantity, morphology, polarity, and viscosity, along with changes in lysosomal protein expression. These factors contribute to tumor progression, metastasis, invasion, and angiogenesis, and most importantly, they inhibit apoptosis in cells [13]. Crucially, lysosomal overproduction and hyperactivity can sequester anticancer drugs and toxins, shielding tumor cells from therapeutic effects [14]. Furthermore, lysosomes enhance cancer cell survival and therapeutic resistance by recycling anticancer treatment-induced damaged macromolecules and organelles through autophagy [15]. Thus, lysosomes exert a crucial part in both cancer development and therapeutic resistance. However, the unique characteristics of tumor lysosomes increase their susceptibility to lysosomal membrane permeabilization (LMP) compared to the normal cells [16,17]. In cases of severe LMP, the lysosomal membrane can rupture, leading to the release of lysosomal contents, including cathepsins and other proteases along with undegraded substrates (like chemotherapy drugs), into the cytoplasm [18,19]. This release can trigger cell death pathways and restore therapeutic function of drugs, toxins or other therapeutic agents contained within the lysosomes. LMP and subsequent lysosomal rupture are now recognized as pivotal in inducing cancer cell death and enhancing therapeutic response [20,21]. Therefore, targeting lysosomes and inducing LMP offers an innovative approach to cancer therapy, potentially overcoming resistance to existing treatments and boosting their effectiveness. As such, lysosomes are a promising target for the development of therapeutic sensitizers.

It should be noted that the development of therapeutic sensitizers capable of specifically targeting tumor and even its cellular organelles while minimizing side effects on normal tissues, could provide more effective strategies to overcome therapeutic resistance in cancer treatments. Current approaches for effectively and specifically inducing lysosome dysfunction in tumor cells are not yet satisfactory, there is an ongoing and immediate requirement for the development of novel theranostic agents [22]. In this circumstance, photodynamic therapy (PDT) stands out due to its remarkably high spatiotemporal precision and controllability, offering an effective solution to tackle therapeutic resistance challenges [23,24]. PDT utilizes light-absorbing photosensitizers (PSs) to produce reactive oxygen species (ROS), which subsequently provoke cancer cell apoptosis and death. The substantial amount of ROS produced can not only directly inflict cell damage and lead to death but also enhance the sensitivity of tumor cells to other treatments, especially radiotherapy [25,26]. The molecular structure of PSs can be designed to selectively target subcellular organelles, such as lysosomes, to amplify precise cellular therapeutic effects [27,28]. Consequently, PDT emerges as a promising approach to address therapeutic resistance, especially considering its non-invasive nature, low systemic toxicity, and the unique characteristic of minimal side effects. Unfortunately, most conventional PSs are susceptible to aggregation-caused quenching (ACQ), a classic phenomenon attributed to the extensive π−π stacking interactions in their aggregated state, leading to significantly reduced fluorescence and ROS production, which severely compromises the applications of PSs in fluorescent imaging and PDT therapy [29,30]. To tackle this issue, Tang and his team introduced aggregation-induced emission (AIE) effect in 2001. AIE, represents a contrasting phenomenon to conventional ACQ, where fluorophores exhibit minimal or negligible emission in dilute solution, yet their luminescence is markedly enhanced upon aggregated state [31,32]. This breakthrough has led to the creation of innovative, highly efficient luminescent probes known as AIEgens [33,34]. Among them, AIE-active PSs exhibit improved optical properties and exhibit robust ROS generation capabilities within aggregated forms [35–37]. These properties render AIE-active PSs ideal candidates for PDT. Considering all relevant factors, it is plausible to envision that developing a new AIE-active PS capable of efficiently producing ROS and specifically disrupting lysosomes could have a huge therapeutic impact. It can not only combat tumors via PDT, but also re-sensitize tumor cells to other therapies, effectively acting as a therapeutic sensitizer. Such a strategy could potentially maximize the therapeutic effect, complement conventional clinical treatments, and ultimately improve the survival rates for patients with cancer.

Herein, we developed a novel AIE-active photosensitizer named QM-DMAC (Scheme 1 and Fig. 1A). It is capable of specifically targeting lysosomes and monitoring changes in lysosome viscosity within living cells under various conditions, such as inflammation and autophagy. Moreover, its ability to effectively distinguish between tumor and normal cells can significantly facilitate cancer diagnostics. Additionally, it will offer valuable insights into the biological and pathological roles of lysosomal viscosity. Furthermore, with its satisfactory ROS generation capability, QM-DMAC can dramatically induce ROS-mediated LMP and cause lysosome rupture. This property endows QM-DMAC with the ability to specifically ablate tumors via PDT and restore the sensitivity of cancer cells to radiotherapy and chemotherapy, thereby enhancing the therapeutic effect and acting as an excellent therapeutic sensitizer. By integrating PDT with conventional clinical treatment (chemotherapy and radiotherapy), QM-DMAC can exert a potent tumor-eliminating effect (Scheme 1). Therefore, this study possesses significant potential in directing the advancement of therapeutic sensitizers and to further promote tumor theranostics.

2. Results and discussion

2.1. Synthesis and photophysical properties

The molecular structure and synthetic route of QM-DMAC are depicted in Fig. 1A, while the corresponding synthetic procedures and characterization data are available in the supplementary material. In brief, QM-DMAC was obtained by the Knoevenagel condensation of 2-(1,2-dimethylquinolin-4(1H)-ylidene)malononitrile (**1**) with 4-(9,9-dimethylacridin-10(9H)-yl)benzaldehyde (**2**). QM-DMAC has a D–π–A structure, in which the AIE-active quinoline–malononitrile unit serves as the electron acceptor (A) [38] 9,9-dimethyl-9,10-dihydroacridine unit is chosen as the electron donor (D) [39] while the carbon-carbon double bond and benzene ring are used to extend the π conjugation. The D–π–A

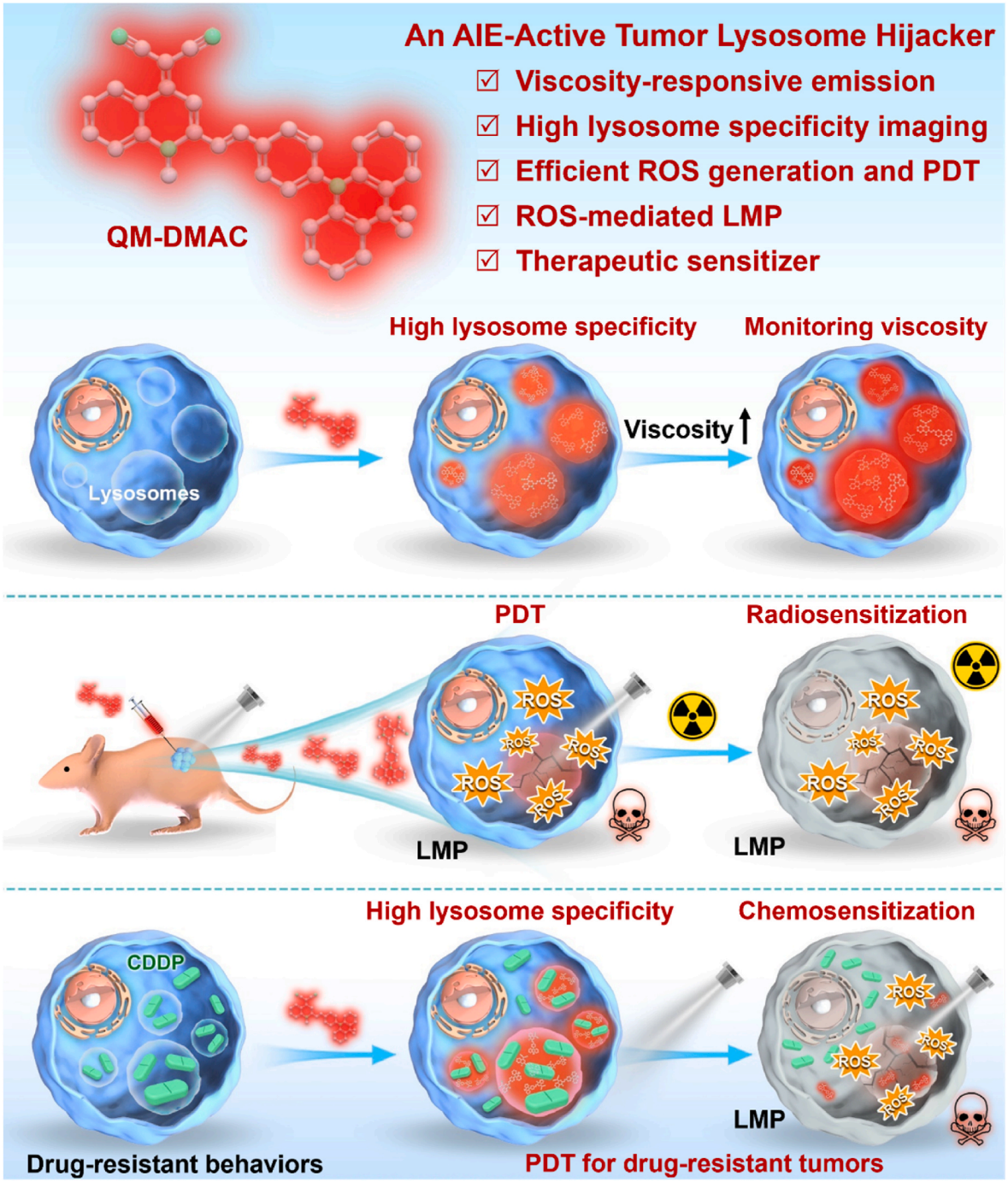

Scheme 1. Schematic illustration of a novel aggregation-induced emission (AIE)-active tumor lysosome hijacker, QM-DMAC, which enables specific visualization of tumor lysosomes and generates a substantial amount of reactive oxygen species (ROS) in tumor cells under white light irradiation. This process precisely induces ROS-mediated lysosomal membrane permeabilization (LMP) and subsequent lysosomal damage. Consequently, this approach effectively boosts photodynamic therapy (PDT) efficacy, restores the sensitivity of tumor cells to treatment, overcomes therapeutic resistance, and enhances the synergistic therapeutic effects when PDT is integrated with conventional radiotherapy or chemotherapy. CDDP for cisplatin.

structure is beneficial for intramolecular electron transfer (ICT), acquiring a low electronic bandgap (E_g), and a small energy gap between the singlet (S_1) and triplet (T_1) states (ΔE_{ST}) that is desirable for highly efficient photosensitizers [40].

QM-DMAC shows an absorption maximum at 445 nm in dimethyl sulfoxide (DMSO) solution (Fig. 1B), which is associated with the ICT. To verify the AIE activity of QM-DMAC, fluorescence spectra in DMSO/water mixtures with different water fractions (f_w) were recorded. DMSO and water serve as good and poor solvents, respectively. As shown in Fig. 1C and D, QM-DMAC is weakly fluorescent in DMSO and at relatively low water fractions ($f_w \leq 40$ %), while the fluorescence intensities increase significantly with higher water fractions, and an approximately 11-fold enhancement of fluorescence (peaking at 607 nm) is observed when the water fraction reaches 90 %, suggesting the AIE properties of QM-DMAC. The weak fluorescence of QM-DMAC when $f_w \leq 40$ % is mainly due to the dissipation of excited state energy through non-radiative channel of intramolecular motions, whereas aggregates forming with the increase of water fractions restricts intramolecular motions

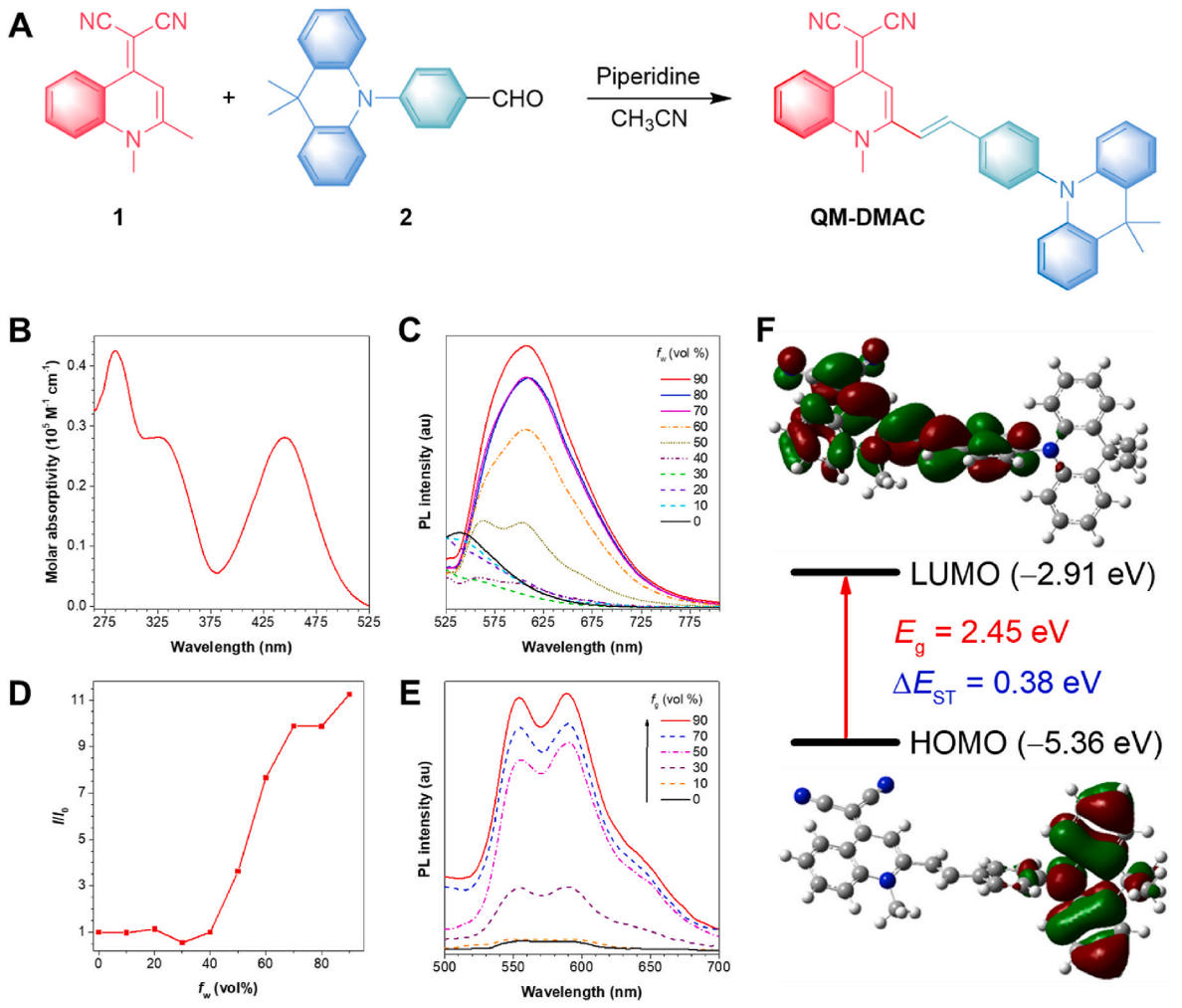

Fig. 1. (A) Synthetic route of QM-DMAC. (B) Molar absorptivity of QM-DMAC in DMSO solution (10^{-5} M). (C) Photoluminescence spectra of QM-DMAC in DMSO/water mixtures with different water fractions (f_w), λ_{ex} = 445 nm. (D) Plot of relative fluorescence (I/I_0) of QM-DMAC versus water fractions in the DMSO/water mixtures. (E) Photoluminescence spectra of QM-DMAC in DMSO/glycerol mixtures with different glycerol fractions (f_g); λ_{ex} = 445 nm. (F) Frontier orbital distributions, energy levels, and energy gap between the singlet (S_1) and triplet (T_1) states ($\triangle E_{ST}$) for QM-DMAC.

and promotes the radiative channel, thereby enhancing luminescence [41]. In addition, the response of QM-DMAC to viscosity has also been studied. Glycerol is a highly viscous liquid that can be used to mimic viscous conditions of inhibiting intramolecular motions [42]. Fig. 1E illustrates the fluorescence changes of QM-DMAC in DMSO/glycerol mixtures with different glycerol fractions (f_g), and gradual fluorescence enhancement can also be found with the increase of glycerol fractions, especially when $f_g > 50$ %, further verifying the AIE characteristics of QM-DMAC.

2.2. ROS generation

To further explore the ROS generation properties of QM-DMAC, 2′,7′-dichlorofluorescin diacetate (DCFH-DA) was used as an indicator of the total ROS generation efficiency. As shown in Fig. S3A, after light irradiation, the fluorescence intensity of DCFH-DA alone remained unchanged. In the presence of QM-DMAC after light irradiation, the fluorescence intensity of DCFH-DA increased by 95-fold. Nonetheless, commercially available photosensitizer Chlorin e6 (Ce6) showed a very low ROS generation efficiency (14-fold). These results suggest the high total ROS generation efficiency of QM-DMAC. Subsequently, we utilized hydroxyphenyl fluorescein (HPF) and Dihydrorhodamine 123 (DHR 123) to assess the production of hydroxyl radicals (•OH) and superoxide anions ($O_2^{-\bullet}$), respectively. As illustrated in Figs. S3C and 3D, the fluorescence intensity of HPF or DHR 123 alone did not change after white light illumination. In the presence of QM-DMAC, the fluorescence intensity of HPF and DHR 123 gradually increased by 25-fold and 112-fold, respectively, after light irradiation. This demonstrates that QM-DMAC significantly enhances the generation of •OH and $O_2^{-\bullet}$. In addition, 9,10-anthracenediyl-bis(methylene)dimalonic acid (ABDA) was used to assess the production of singlet oxygen ($^1O_2$). As illustrated in Fig. S3B, the absorbance of the QM-DMAC + ABDA solution remained almost unchanged when exposed to white light, demonstrating a lower capability for $^1O_2$ generation. Generally, ROS can be categorized into two distinct types: Type I ROS, which include •OH and $O_2^{\bullet-}$, are produced through electron transfer processes; and Type II ROS, which include $^1O_2$, are generated via energy transfer processes. The $^1O_2$ is generally identified as the dominant species for PDT due to its stronger interactions with biological substrates. However, the production of $^1O_2$ through the Type II mechanism is highly dependent on the presence of oxygen. In contrast, Type I PSs have low oxygen dependence, as they avoid direct and rapid depletion of O_2 during PDT, making them promising candidates for the treatment of hypoxic tumors. Based on the above results, QM-DMAC exhibits high efficiency in generating Type I ROS.

2.3. Theoretical calculations

Density functional theory and time-dependent density functional theory calculations were executed at the B3LYP/6-311G(d, p) level using Gaussian 16 package, to study the electronic property and the energy gap between the singet S_1 and T_1 states (ΔE_{ST}) of QM-DMAC, respectively. As shown in Fig. 1F, the highest occupied molecular orbital (HOMO) and lowest unoccupied molecular orbital (LUMO) are distributed in a distinctly separated fashion, with a small energy gap (E_g) of 2.45 eV. The HOMO is predominantly located on the electron-donating 9,9-dimethyl-9,10-dihydroacridine unit, whereas the LUMO is distributed in the electron-withdrawing quinoline–malononitrile unit and extends to the benzene ring through carbon-carbon double bond, indicating the presence of ICT effects, which contributes to reducing ΔE_{ST} and thus efficient ISC process. Additionally, the experimental results have shown that QM-DMAC has a good ROS generation ability, further confirming that efficient ISC process occurs.

Interestingly, QM-DMAC exhibits high efficiency in generating Type I ROS, that is to say, QM-DMAC is mainly a Type I photosensitizer, prompting us to further gain insights into the underlying determinants. It is worth mentioning that a small ΔE_{ST} and a reduced T_1 energy level are favorable factors for the generation of Type I ROS, the former facilitates effective ISC process and the latter inhibits the energy transfer to O_2, which is conducive to Type I ROS generation. However, a lower triplet energy level may lead to a larger ΔE_{ST}, which is unfavorable to the ISC process [7,43,44]. As for QM-DMAC, the calculated excited state energies of S_1 and T_1 are 2.02 eV and 1.64 eV, respectively, having a relatively small ΔE_{ST} value of 0.38 eV and low T_1 energy level. Combing with the experimental results, we consider that QM-DMAC possesses a suitable ΔE_{ST} and T_1 energy level to favor the Type I ROS generation pathway (Fig. S4).

2.4. Lysosome-specific cell imaging

Motivated by the distinctive AIE properties of QM-DMAC, we further investigated its potential biological applications in tumor theranostics. Accordingly, we initially performed live-cell imaging of QM-DMAC using the A549 tumor cell line, followed by analysis using confocal microscopy. The incubation of A549 cells with QM-DMAC for 60 min resulted in bright red fluorescence in the cellular cytoplasm (Fig. S5), indicating good cellular permeability and high-contrast cell imaging ability. To determine the subcellular distribution specificity of QM-DMAC, the colocalization test was conducted by staining A549 cells with QM-DMAC and subsequently co-incubated them with Lysotracker Deep Red (LTDR), a commercial lysosome-targeting probe. As shown in Fig. 2A, a good fluorescent overlap is observed between the QM-DMAC and the LTDR, with a high Pearson's correlation coefficient of 0.86. This indicates that QM-DMAC is capable of selectively accumulating with lysosomes of A549 cells, highlighting its lysosome-targeted bioimaging ability. Additionally, other cell lines, including 4T1 cells and HeLa cells, were also used to carried out colocalization experiments, and the results further confirm that QM-DMAC exhibits superior lysosomes specificity (Fig. S6).

Lysosomes serve as sophisticated hubs for cellular signalling, metabolism, and quality control, playing a crucial role in the regulation of substance internalization and trafficking [17]. Undoubtedly, the hydrophobic QM-DMAC is neither a lysosomal enzyme substrate, nor possesses typical lysosomal targeting moieties, e.g., *N*,*N*-dimethyl amino and morpholine. Considering its lysosome-specific staining characteristic, we presume that the formation of nanoaggregates of QM-DMAC makes a significant contribution to its cellular uptake. The formation of aggregates was well characterized using dynamic light scattering (DLS). The data demonstrated the formation of aggregates with nanoparticles averaging 106 nm in size (Fig. S7). We presume that these small aggregates are likely to facilitate subsequent cellular uptake, potentially entering cells through lysosome-mediated endocytosis while remaining

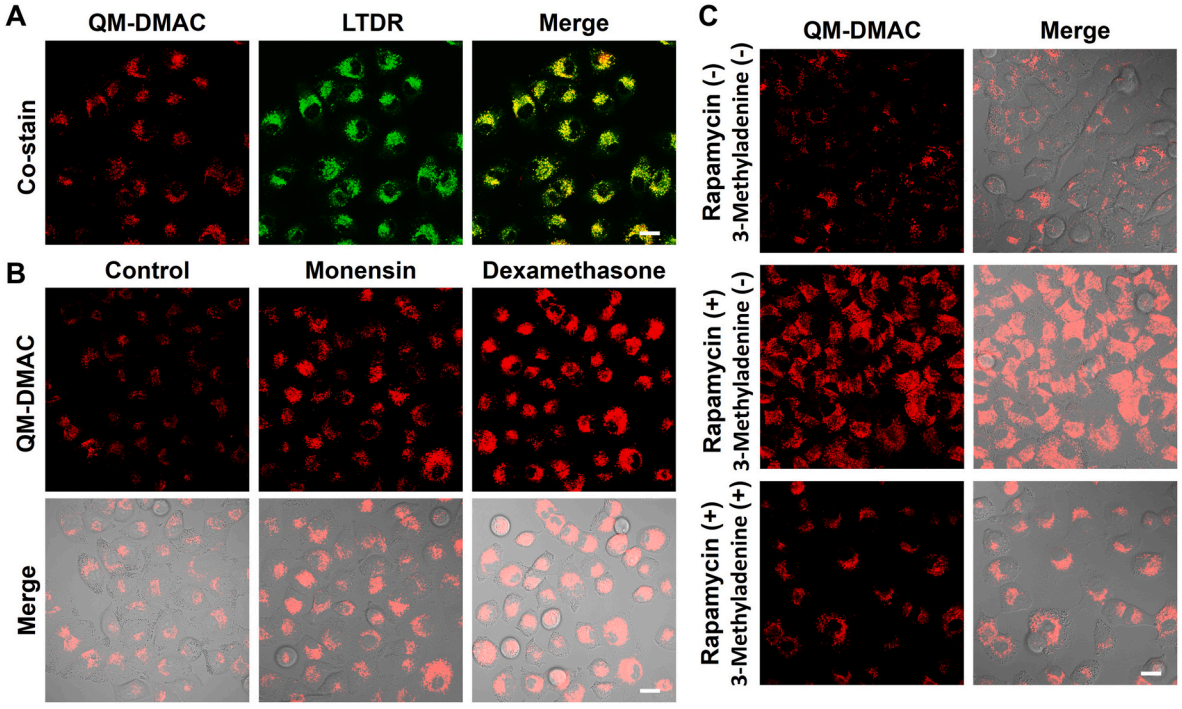

Fig. 2. (A) The co-localization imaging showed A549 cells stained with QM-DMAC and Lysotracker Deep Red (LTDR), and their merged images. Inset: Calculated Pearson's colocalization coefficient (R). (B) Fluorescence images and merge images of A549 cells treated with monensin (pre-treated, 20 μM), or dexamethasone (post-treated, 100 μM) and stained with QM-DMAC (20 μM) for 60 min. (C) Confocal imaging of A549 cells pre-incubated with or without rapamycin (10 μg/mL) and 3-Methyladenine (100 μM), then stained with QM-DMAC. Scale bar = 20 μm. (For interpretation of the references to colour in this figure legend, the reader is referred to the Web version of this article.)

in an aggregate form [12].

Based on the above results, the viscosity response and lysosome-specific targeting abilities of QM-DMAC endow it with the potential to assess lysosomal viscosity within living cells. Subsequently, we utilized QM-DMAC to validate its lysosome-specific viscosity-responsive properties in A549 cells. To modulate intracellular viscosity, we introduced the antifungal drugs monensin and nystatin, both of which are known to increase intracellular viscosity and induce cellular dysfunctions. A549 cells were first cultured with or without monensin or nystatin for 40 min, respectively, after washing, it stained with QM-DMAC for another 60 min. As illustrated in Fig. 2B and S8, stronger red fluorescence emissions are observed in A549 cells, which were pre-treated with monensin or nystatin. This enhancement in fluorescence aligns with the results from solution-based experiments, and is likely due to the viscosity-increasing effects of monensin or nystatin within living cells. The elevated viscosity likely restricts the intramolecular motions of QM-DMAC, consequently resulting in a significant fluorescence enhancement. To substantiate the viscosity-responsive behavior of QM-DMAC for monitoring changes in lysosomal viscosity, we initially incubated A549 cells with QM-DMAC, and then dexamethasone, a clinical drug known to increase intracellular viscosity, was added. As depicted in Fig. 2B, fluorescence enhancement was observed in A549 cells pre-stained with QM-DMAC, following the addition treatment of dexamethasone. Therefore, QM-DMAC can be effectively utilized for detecting changes in lysosomal viscosity of living cells. Lysosomal viscosity, a critical determinant of cellular microenvironment stability, plays a significant role in elucidating the intricate link between lysosomal state and cellular health. Understanding its relationship is essential for assessing cell status, facilitating early diagnosis, and enabling effective monitoring of a spectrum of diseases [45]. The inflammation triggers a rise in the viscosity of the intracellular environment. Consequently, we utilized lipopolysaccharide (LPS) [46], a well-established inflammation-inducing agent, to stimulate an inflammatory cell state change and subsequently evaluate QM-DMAC's capacity to monitor lysosome viscosity changes under pathological conditions. A549 cells were initially cultured with LPS for 2 h, followed by a 60 min stained with QM-DMAC. In stark contrast to the control cells, A549 cells pre-cultured with LPS exhibit significantly brighter fluorescence signals (Fig. S8). These results clearly demonstrate that QM-DMAC effectively monitors the intracellular viscosity changes induced by LPS.

Autophagy, a lysosomal degradation pathway, is essential for cellular health as a critical catabolic process. Dysregulation of autophagy, ranging from inhibition to excessive activation, is associated with a spectrum of severe diseases [47]. Considering the distinct internal microenvironments of lysosomes and autophagosomes, lysosomal viscosity is expected to exhibit significant fluctuations during autophagy. To track these changes, we utilized the lysosomal viscosity-responsive probe QM-DMAC, which allows for the assessment of lysosomal viscosity changes. Initially, we induced autophagy using rapamycin, a well-known inducer of autophagy, which has been reported to induce substantial viscosity changes during pharmacologically induced autophagy [48]. Fig. 2C and S9 illustrate that pre-treatment with rapamycin induces autophagy in A549 cells, leading to elevated lysosomal viscosity and a corresponding enhancement in QM-DMAC fluorescence. The subsequent addition of autophagy inhibitor, 3-methyladenine (3-MA), effectively suppressed rapamycin-induced autophagy. Consequently, no further increase in fluorescence was observed, and lysosomal viscosity remains stable. These findings suggest that QM-DMAC, a lysosomal viscosity-responsive probe, serves as a reliable tool for monitoring cellular autophagy by visualizing changes in lysosomal viscosity. Furthermore, recent studies have indicated that lysosomal viscosity is elevated in tumor cells compared to normal cells, which could serve as a potential biomarker for tumor detection [49]. Thus, constructing responsive and precise fluorescent probes for assessing cellular viscosity can markedly improve cancer diagnostics and offer valuable insights into the role of viscosity in biological and pathological contexts.

To broaden the application of QM-DMAC, we utilized the lysosomal viscosity-responsive probe QM-DMAC to stain both tumor and normal cell lines, thereby evaluating its potential for specifically visualizing tumor cells. Fig. S10 illustrates that after staining with QM-DMAC for 60 min, tumor cells (4T1, A431, Cal-27 and HeLa) display stronger fluorescence intensity than normal cells (NIH3T3, 16HBE, HT22 and NCM460). These results show that the lysosomal viscosity-responsive probe QM-DMAC can effectively discriminate between tumor and normal cells.

2.5. ROS-mediated lysosomal membrane permeabilization

The lysosome-targeting capability and excellent optical properties of QM-DMAC encouraged us to further investigate its application in biological research. As mentioned above, QM-DMAC has a relatively small ΔE_{ST} (0.38 eV), which contributes to efficient ISC process and ROS generation, then we subsequently evaluated the ROS generation triggered by white light irradiation of QM-DMAC within A549 cells using the ROS indicator DCFH-DA (2,7-dichlorodihydrofluorescein diacetate). The subsequent increase in fluorescence of the indicator upon cellular ROS oxidation confirms the intracellular ROS generation. A substantial increase fluorescence signal was recorded in A549 cells cultured with QM-DMAC and DCFH-DA after white light irradiation (QM-DMAC + L), whereas the control and QM-DMAC alone groups exhibit no significant fluorescence enhancement (Fig. 3A). Furthermore, pre-treatment of A549 cells with the ROS scavenger N-acetylcysteine (NAC) for 1 h, followed by incubation with QM-DMAC and subsequent white light irradiation (QM-DMAC + L + NAC), displayed no significant increase in fluorescence signals, indicating that NAC can effectively counteract the ROS increase induced by QM-DMAC and light. These findings demonstrate that QM-DMAC can generate a substantial amount of ROS in cells upon white light illumination, highlighting its potential as a PS for PDT. Subsequently, we evaluated the therapeutic effects of QM-DMAC on tumor cells (A549) and normal cells (16HBE) using the 3-(4,5 dimethylthiazol-2-yl)-2,5-diphenyltetrazolium bromide (MTT) assay. Following a 24 h staining with QM-DMAC in the absence of light, the viability of both tumor and normal cells remained above 95 %, even at concentrations up to 30 μM, suggesting that QM-DMAC exhibits negligible cytotoxicity in the dark (Fig. 3B and C). Under white-light irradiation, 16HBE normal cells maintain a viability close to 90 % (Fig. 3B). In contrast, under the same irradiation conditions, A549 tumor cells exhibit dose-dependent cytotoxicity, with a progressive decrease in cell viability with increasing concentrations, and 20 μM concentration of QM-DMAC results in significant cell death (Fig. 3C). Furthermore, the MTT results also demonstrated that the light-induced toxicity of QM-DMAC to A549 cells can be mitigated by NAC pre-treatment (Fig. 3D). Our previous results indicate that the lysosomal viscosity-responsive probe QM-DMAC exhibits reduced responsiveness to the lower lysosomal viscosity characteristic of normal cells, potentially influencing the subsequent light-induced cytotoxic effect. Considering the specific anticancer activity of QM-DMAC, it is reasonable to conclude that QM-DMAC can serve as a PS and effectively target tumor lysosomes, which exhibit higher viscosity. This selective targeting ability leads to a significant increase in intracellular ROS levels upon white light irradiation, thereby triggering specific anticancer effects.

Drawing from the results presented, we hypothesize that selective targeting of QM-DMAC in tumor cell lysosomes, combined with white light-induced ROS generation, could induce LMP, which can disrupt the lysosomal membrane's integrity and result in tumor cell death. To verify this hypothesis, we applied established lysosomal integrity indicators, acridine orange (AO) and FITC-Dextran, to evaluate the lysosomal membrane integrity in A549 cells. Typically, AO displays red fluorescence within lysosomes and emits green fluorescence in the cytoplasm or nucleus. Disruption of the lysosomal membranes results in a significant reduction in AO's red fluorescence (Fig. 3E). As shown in Fig. 3F, both green fluorescence in the cytosol/nucleus and red fluorescence in the

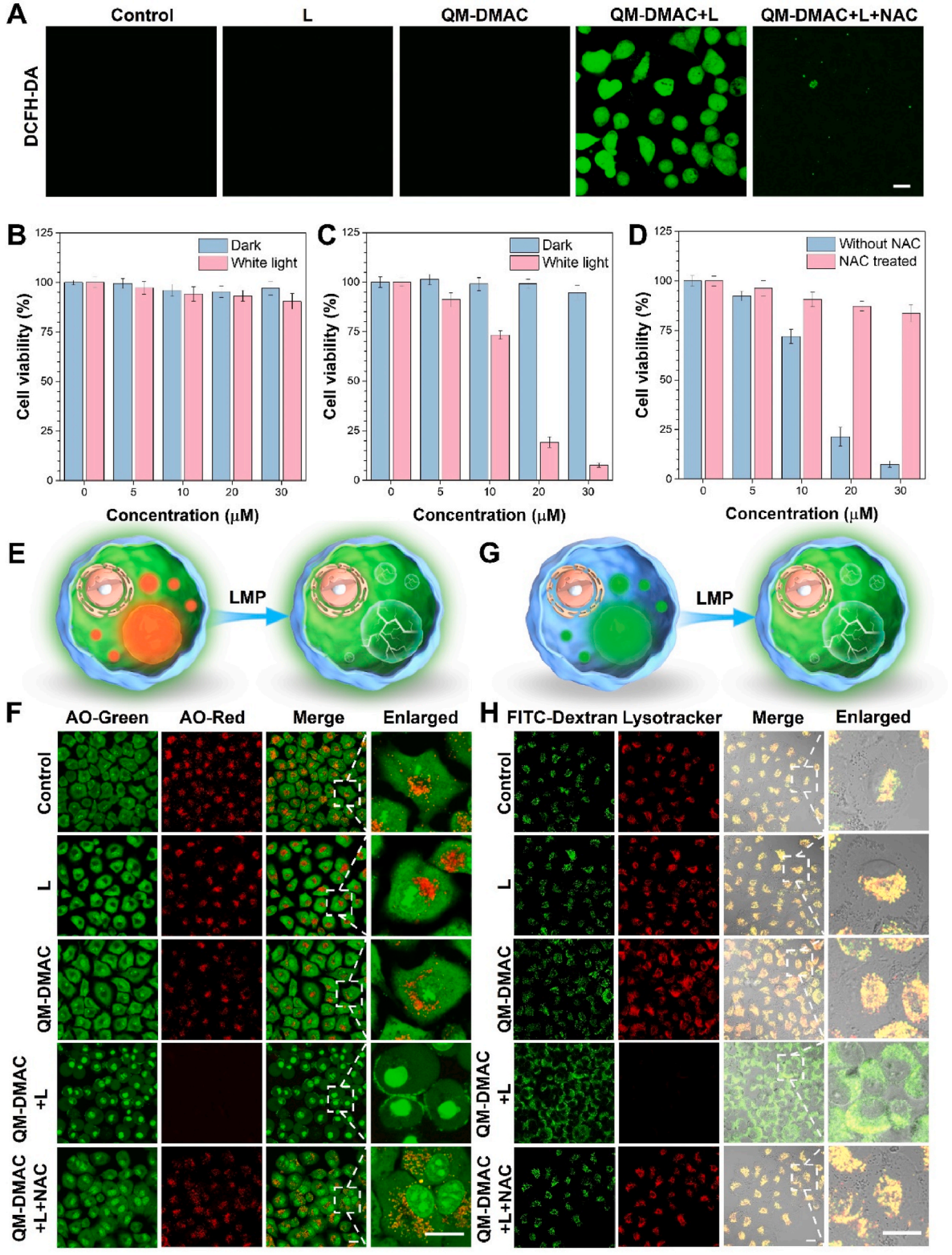

Fig. 3. (A) Fluorescence images of intracellular ROS generation in A549 cells. L for white light irradiation. (B) The cell viability assessment of 16HBE cells. (C) The cell viability assessment of A549 cells. (D) Cell viability of A549 cells pretreated with N-acetylcysteine (NAC) for 1 h and then incubated with QM-DMAC under dark or white-light irradiation. (E) Illustration of the acridine orange (AO) assay. In normal cells, AO exhibits red fluorescence within lysosomes and shifts to green when it localizes to the cytosol or nucleus. Lysosomal membrane permeabilization (LMP) and lysosomal rupture cause a significant reduction in AO's red fluorescence. (F) A549 cells were subjected to various treatments and then stained with AO for 30 min. (G) Illustration of FITC-dextran assay. Briefly, when normal cells are incubated with FITC-dextran, the green signal from FITC-dextran is sequestered in the lysosomes. When these cells are subsequently subjected to LMP, the green fluorescence is expected to disperse from the lysosomes throughout the entire cytosol. (H) FITC-Dextran-loaded A549 cells treated with various treatments and then stained with commercial dye Lysotracker Deep Red (LTDR, 50 nM) for co-staining imaging. Scale bar = 20 μm. (For interpretation of the references to colour in this figure legend, the reader is referred to the Web version of this article.)

lysosome are observed in the control, Light (L), and QM-DMAC groups, indicating that lysosomal integrity remained intact. In contrast, A549 cells incubated with QM-DMAC and subsequently exposed to white light irradiation exhibit a marked decrease in AO's red fluorescence intensity, suggesting LMP and lysosomal membrane damage. Additionally, when cells were pre-cultured with NAC, followed by incubation with QM-DMAC and subsequent light irradiation, red fluorescence in the lysosome was re-observed, demonstrating that NAC can mitigate the light-induced lysosomal rupture. In the FITC-Dextran assay, FITC-Dextran is endocytosed and localized within lysosomes, emitting a green fluorescence signal. Upon LMP, the green fluorescence is expected to disperse from the lysosomes throughout the entire cytosol (Fig. 3G). Normally, LTDR accumulation in lysosomes, however, LMP impairs the lysosomal environment and integrity, leading to a decrease in LysoTracker fluorescence. Both the green fluorescence from FITC-Dextran and the red fluorescence from LTDR in the lysosomes are observed in the control, L, and QM-DMAC groups, indicating that lysosomal integrity is maintained (Fig. 3H). In contrast, A549 cells stained with QM-DMAC and subsequently exposed to white light irradiation exhibit a significant reduction in LTDR's red fluorescence intensity, and the green signal from FITC-Dextran escaped from the lysosomes into the cytosol, suggesting that QM-DMAC induces LMP and subsequent damage to the lysosomes. Furthermore, when cells were pre-treated with the NAC, the green and red fluorescence within the lysosomes was re-observed, once again demonstrating that NAC can mitigate the light-induced LMP and lysosomal rupture. As a comparison, we evaluated the ability of the commercially available photosensitizer Chlorin e6 (Ce6) to induce LMP. After white light irradiation, the red fluorescence of AO remains localized to the lysosomal site, as depicted in Fig. S11. Similarly, the fluorescence of FITC-Dextran co-stained with LTDR also remains localized to the lysosomal site after irradiation (Fig. S12). These observations indicate that Ce6 does not induce LMP upon exposure to white light, unlike QM-DMAC. Above all, the lysosomal viscosity-responsive probe QM-DMAC can serve as a PS, inducing ROS-mediated LMP, which compromises the integrity of the lysosomal membranes.

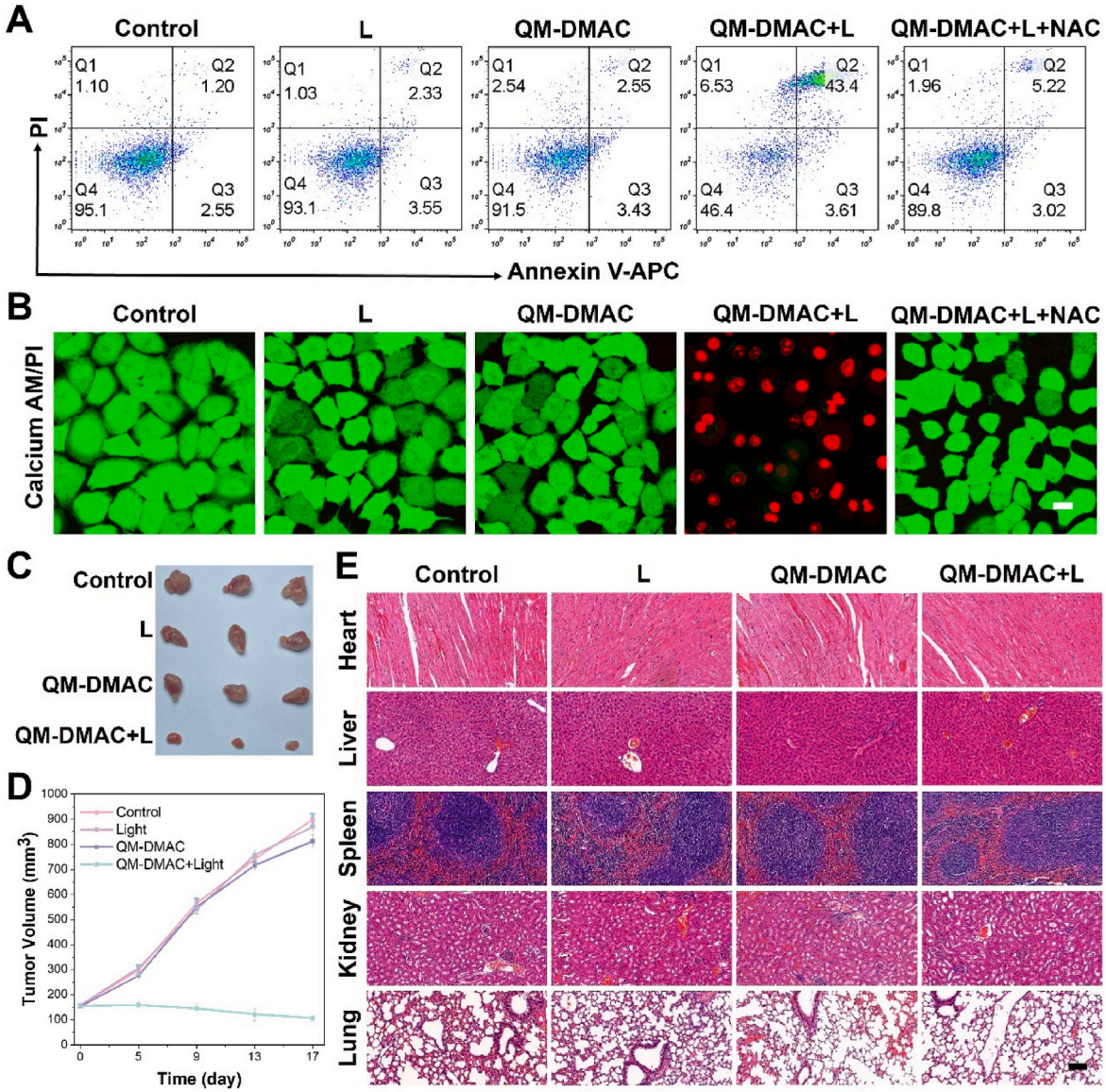

Fig. 4. (A) Annexin V-ACP/PI staining. L: Light. (B) A549 cells treated with QM-DMAC (20 μM) were subjected to a live/dead cell staining (Calcium AM/PI assay). (C) Images of tumors obtained following various treatments. (D) Tumor volume growth curves at various time points. (E) H&E staining of major organs. Scale bar = 100 μm.

2.6. Photodynamic therapy and radiotherapy sensitization

Prior research indicates that LMP or complete lysosomal rupture is highly detrimental. The leakage of lysosomal contents, such as protons and hydrolases, along with the accumulation of undegraded substrates, can severely impair cellular components. Such damage may activate cell death pathways or trigger inflammatory signaling, ultimately leading to cell death [16]. Capitalizing on the effective ROS production and LMP induced by QM-DMAC, we conducted additional studies to evaluate the PDT effects of QM-DMAC on tumor cells. The Annexin V-APC/propidium iodide (PI) staining was carried out to analyze apoptosis and elucidate the mechanisms of cell death. It turned out that approximately 53.54 % of tumor cells experienced apoptosis and necrosis after treatment with QM-DMAC combined with white light irradiation (QM-DMAC + L), while other groups exhibited minimal apoptosis. Notably, light-induced apoptosis in the QM-DMAC + L + NAC group was significantly mitigated by ROS scavenger NAC (Fig. 4A and S13). To further visually assess the efficacy of PDT, A549 cells were cultured with Calcium AM/PI to differentiate dead and live cells following various treatments (Fig. 4B). As expected, robust green fluorescence, signifying live cells, was detected in the control, L, QM-DMAC, and QM-DMAC + L + NAC groups, whereas nearly all A549 cells in the QM-DMAC + L group

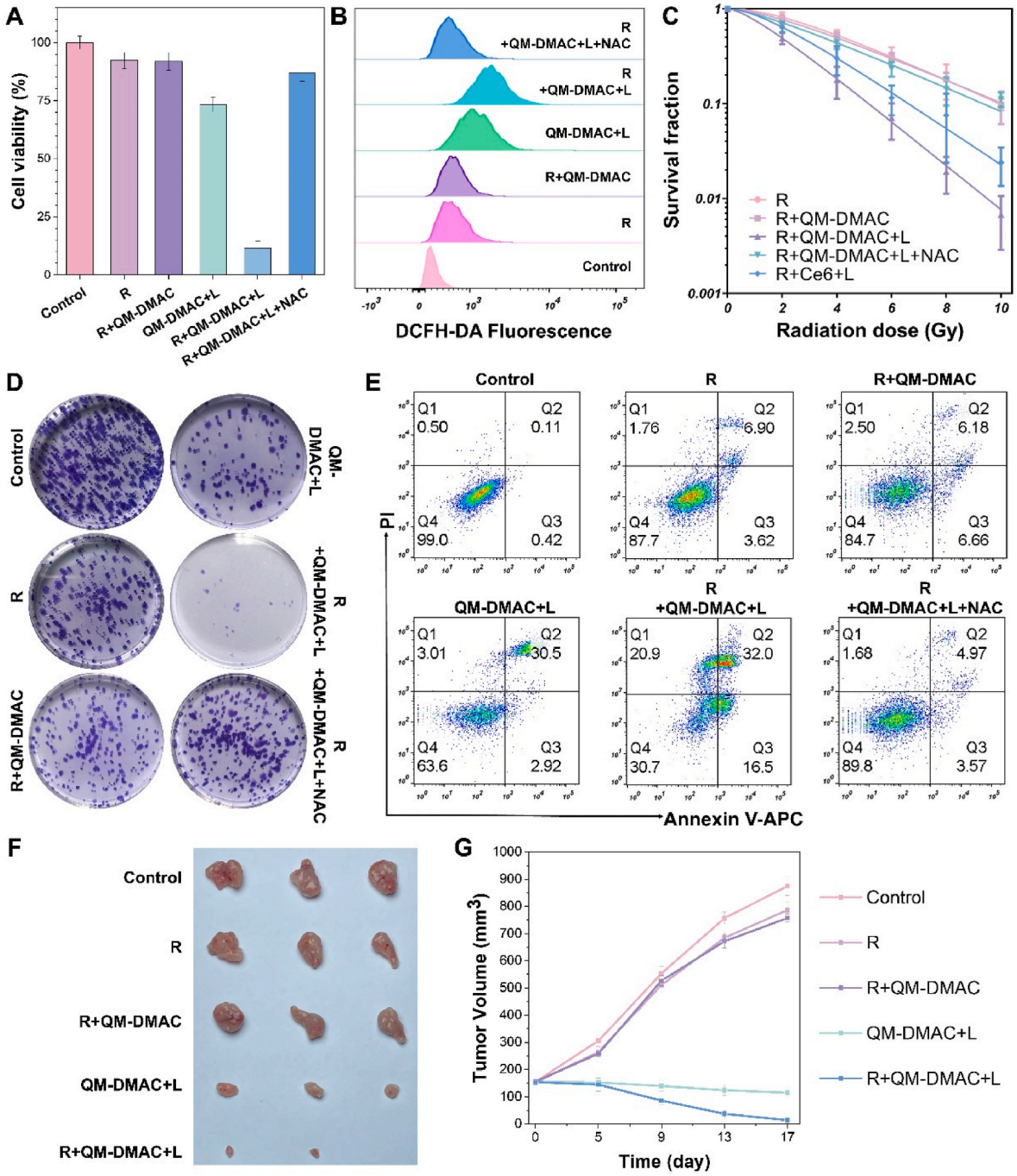

Fig. 5. (A) Cell viability of A549 cells. X-ray (R) for 4 Gy ionizing radiation treatment; L: Light; NAC: N-acetylcysteine. (B) Quantification of cell ROS level using flow cytometric analysis. R: radiation; L: Light; NAC: N-acetylcysteine. (C) Survival curves of A549 subjected to various treatments. R: 4 Gy radiation; L: Light; Ce6: Chlorin e6. (D) Representative photographs of colony formation in A549 cells following various treatment conditions. (E) Annexin V-ACP/PI staining. (F) Images of tumors obtained following various treatments. R: radiation; L: Light. (G) Tumor volume growth curves.

displayed distinct red fluorescence, signifying substantial cell death. These results demonstrate that QM-DMAC possesses high efficacy for the ablation of tumor cells via the PDT pathway.

Encouraged by QM-DMAC's exceptional performance in cellular PDT experiments, we proceeded to evaluate its phototherapeutic efficacy *in vivo* using A549 tumor-bearing BALB/c nude mice. Fig. 4C and D illustrate that treatment with white light (L) or QM-DMAC alone had negligible impact on tumor growth, suggesting that neither light irradiation alone nor QM-DMAC without light exerted a significant antitumor effect. By contrast, combination of QM-DMAC and light (QM-DMAC + L) demonstrated pronounced inhibition of tumor growth compared to the rapid growth observed in the control group. Hematoxylin and eosin staining (H&E), as illustrated in Fig. 4E, no significant tissue damage or inflammation in the major organ across treatment groups. Collectively, these results lead to the compelling conclusion that QM-DMAC, with its excellent biocompatibility and minimal side effects, is highly effective for PDT in A549 tumors.

In radiotherapy, ROS are crucial for inducing cell death through radiation. However, the radioresistance of tumor cells or insufficient ionizing energy during radiotherapy often leads to inadequate ROS generation, which severely limits the efficacy of radiotherapy [50]. While more powerful ionizing radiation can enhance tumor treatment, it also significantly increases damage to normal tissues. Directly enhancing ROS production is an alternative approach to improving radiosensitivity. By boosting cellular ROS levels, one can amplify cellular damage and enhance the cellular response to radiation [51]. The AIE photosensitizer QM-DMAC, upon exposure to white light irradiation, generates a substantial amount of ROS and triggers LMP and lysosomal rupture, thereby exhibiting an effective PDT effect. This motivated us to investigate whether QM-DMAC has the potential to enhance radiosensitivity and serve as a radiosensitizer. Initially, we assessed the viability of A549 cells post-treatment with "combined therapy" (R + QM-DMAC + L), which involves PDT in combination with low-dose radiation therapy (R), using the MTT assay (Fig. 5A and B). The viability of A549 cells in the R + QM-DMAC + L is markedly reduced compared to the other treatment groups (Fig. 5A). Additionally, the level of ROS in the R + QM-DMAC + L group exceeded that of the other groups (Fig. 5B). Those results indicate that upon light irradiation, QM-DMAC can be used to boost cellular ROS generation and enhance the tumor-killing efficacy of radiotherapy. Furthermore, pre-treatment with NAC resulted in no considerable decline in cell viability, and there was minimal escalation in ROS levels. The ROS scavenger is able to reverse the efficacy of the combined therapy (Fig. 5A and B). Next, a clonogenic survival assay was performed to evaluate the potential of QM-DMAC to enhance radiosensitivity. In this assay, A549 cells were pre-cultured with QM-DMAC and then irradiated with white for 0.5 h to generate substantial ROS. After that, cells were subject to graded doses (0, 2, 4, 6, 8, and 10 Gy) of ionizing radiation. The colony-forming ability of A549 cells was evaluated using survival curves (Fig. 5C). The sensitizer enhancement ratio (SER) of the combined therapy (R + QM-DMAC + L) was calculated to be 1.75, which exceeds those of the other treatments. The SER value of the conventional photosensitizer Ce6 (R + Ce6+L) was also determined. It was calculated to be 1.45, suggesting that QM-DMAC outperforms Ce6 in terms of the radiosensitizing effect. This may be due to the fact that QM-DMAC not only produces large amounts of ROS but can also trigger LMP. The ROS scavenger NAC significantly mitigated the synergistically enhanced radiosensitizing effect of QM-DMAC, in which SER value was calculated to be only 0.95. This finding suggests that elevating the cellular ROS level is crucial for enhancing the radiosensitizing effect of QM-DMAC. The clonogenic assay data, in conjunction with the SER values, demonstrate that the combined therapy of R + QM-DMAC + Light exhibits a markedly potent suppressive effect on colony formation compared to radiation (R) or QM-DMAC + L (Fig. 5D).

Additionally, we utilized Annexin V-APC/PI staining to detect apoptosis. Fig. 5E illustrates that radiotherapy (R) alone results in 12.3 % apoptosis; however, when A549 cells were treated with QM-DMAC + L or the combined therapy (R + QM-DMAC + L), there was a notable rise in the rate of apoptotic cell death. Particularly, approximately 69.3 % of A549 tumor cells undergo apoptosis and necrosis following the combined therapy (R + QM-DMAC + L). These findings further demonstrate that, upon white light irradiation, QM-DMAC significantly enhances the radiotherapeutic effect by inducing ROS production and accelerating apoptosis, indicating its considerable capacity as a potent radiosensitizer. Further, we expanded our study to evaluate the *in vivo* radiotherapy sensitization efficacy of QM-DMAC using A549 tumor-bearing mice. The tumor volumes in the QM-DMAC + L and combined therapy (R + QM-DMAC + L) groups are significantly reduced compared to the control mice. Besides, the combined therapy group exhibited notably heightened antitumor activity, revealing that QM-DMAC significantly enhances the anticancer effect of radiotherapy upon white light irradiation (Fig. 5F and G). Thus, these results undoubtedly reinforced the potential of QM-DMAC as an effective radiosensitizer.

2.7. Chemosensitization efficacy and in vivo therapy of drug-resistant tumors

Typically, lysosomes within cells serve as crucial barriers to drugs and toxic materials, effectively resisting the invasion of foreign elements and decomposing or expelling toxic materials within the cells [11]. In particular, within tumor cells, lysosomes are often overexpressed, which can further insulate antitumor drugs from the cytoplasm and shield them from their functional target sites. This sequestration of drugs prevents them from exerting their cytotoxic effects effectively, thereby enhancing tumor drug resistance. The suppression of lysosomes can effectively sensitize cancer cells to chemotherapy, making lysosomes an attractive target for chemotherapy sensitization [52]. Encouraged by QM-DMAC's lysosome-specific targeting, its exceptional ROS generation, effective ROS-mediated LMP, and radiosensitization efficacy, we expanded our investigation to explore the chemosensitization effect of QM-DMAC.

Cisplatin (CDDP), a platinum-based chemotherapeutic agent widely utilized in clinical practice for treating various malignancies, frequently faces challenges in therapeutic efficiency due to the widespread emergence of resistance among cancer cells, a process in which lysosomes are believed to play a significant role [53,54]. We utilized cisplatin-resistant A549 cells (A549/DDP) to examine the chemosensitization effect of QM-DMAC. Accordingly, we initially performed live-cell imaging of QM-DMAC using multidrug-resistant A549/cisplatin (A549/DDP) cells to evaluate its targeting ability toward drug-resistant tumor cells. As shown in Figs. S14 and S15, QM-DMAC exhibits good cellular permeability and high-contrast lysosome-targeted bioimaging ability for drug-resistant A549/DDP cells. Upon white light irradiation, A549/DDP cells exhibited dose-dependent cytotoxicity (Fig. 6A). Most importantly, after treatment with "combined therapy" (CDDP + QM-DMAC + L), which involves PDT in combination with cisplatin treatment (CDDP), the cell viability of A549/DDP in the CDDP + QM-DMAC + L showed a significantly reduced level compared to the other groups, and the level of ROS generation was elevated (Fig. 6B and C). These results indicate that, upon light irradiation, QM-DMAC can be used to boost cellular ROS generation and enhance the tumor-killing efficacy of CDDP treatment against drug-resistant tumor cells. Furthermore, the ROS scavenger was able to reverse both the tumor-killing efficacy and ROS generation induced by the combined therapy (CDDP + QM-DMAC + L + NAC), indicating that the cellular ROS level is crucial for enhancing the chemotherapeutic effect (Fig. 6B and C). LMP compromises the integrity of lysosomal membranes, resulting in the leakage of lysosomal contents. This process enables sequestered antitumor drugs within lysosomes to be released, thereby restoring their original antitumor effects. Consequently, we evaluated QM-DMAC's capacity to induce LMP in drug-resistant A549/DDP cells. Both green fluorescence in cytosol/nucleus and red fluorescence in lysosomes are observed in the control, CDDP, and CDDP + QM-DMAC groups, indicating that lysosomal

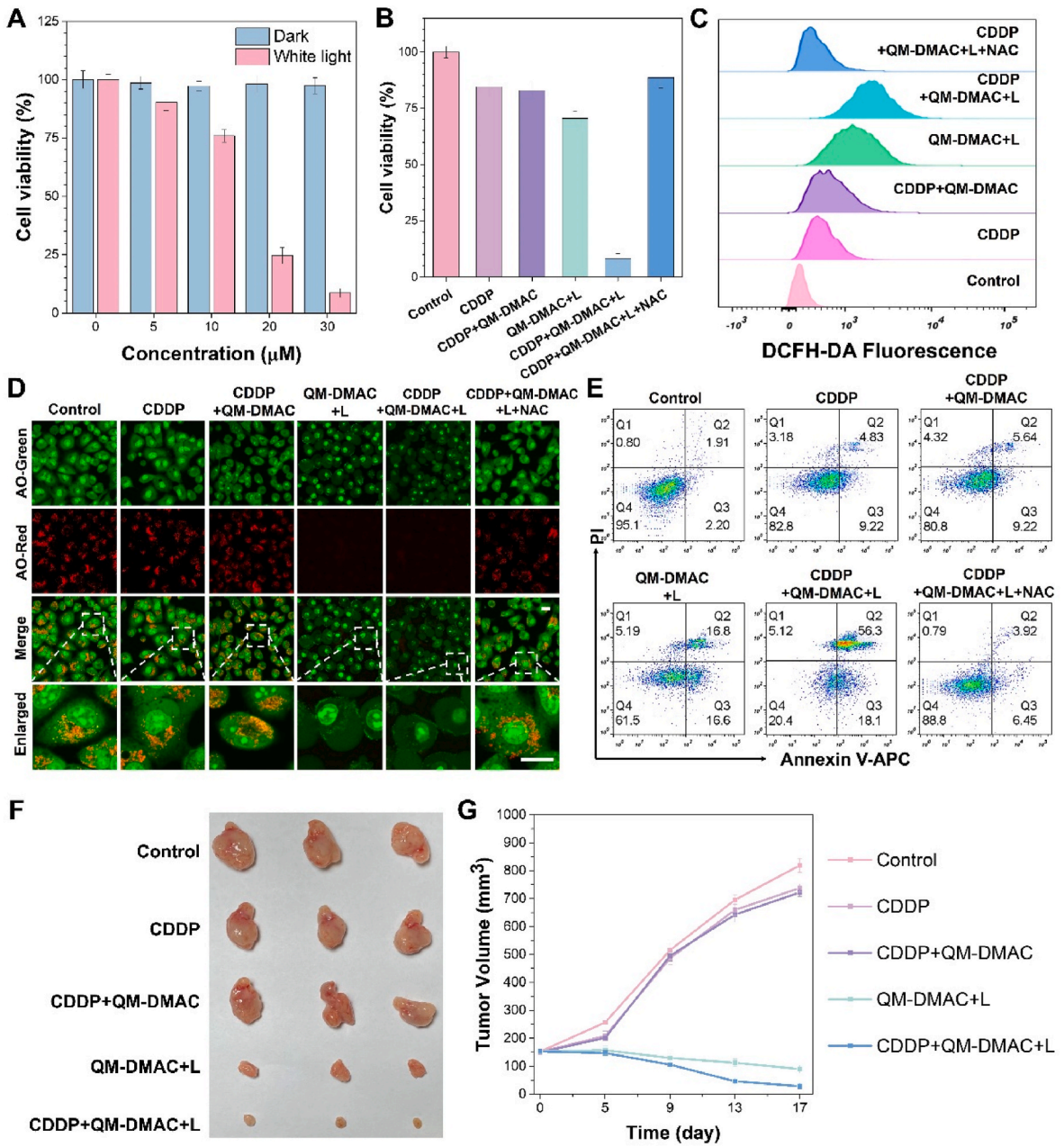

Fig. 6. (A) Cell viability of A549/DDP cells. (B) Cell viability of A549/DDP cells subjected to various treatments. L: Light. Cisplatin: CDDP. NAC: N-acetylcysteine. (C) Quantification of ROS level in A549/DDP cells utilizing flow cytometry. (D) The AO staining for A549/DDP cells. (E) Annexin V-ACP/PI staining of A549/DDP cells. (F) Images of tumors collected from drug-resistant A549/DDP bearing mice. CDDP: Cisplatin; L: Light. (G) Growth curves of tumor volume at different time points in drug-resistant tumors.

integrity is preserved (Fig. 6D). In contrast, QM-DMAC + L and CDDP + QM-DMAC + L groups exhibit a significant reduction in AO's red fluorescence intensity, suggesting LMP and lysosomal membrane damage due to the treatment. Furthermore, NAC is found to mitigate light-induced LMP (Fig. 6D). γ-H2AX, a marker for double-strand breaks, was utilized to assess DNA damage. Following various treatments, drug-resistant A549/DDP cells were immunostained with an Alexa Fluor647 gamma H2A.X antibody and subjected to flow cytometry analysis. Fig. S16 shows that the highest H2A.X fluorescence expression was observed within the combined therapy (CDDP + QM-DMAC + L). These results suggest that QM-DMAC can generate a substantial amount of ROS and trigger LMP in drug-resistant cells upon white light irradiation, resulting in the disruption of lysosomal membrane integrity and the subsequent release of lysosomal-stored CDDP into the cytoplasm. This release may, in turn, cause significant DNA damage and restore the therapeutic function of CDDP. Subsequently, we employed Annexin V-APC/PI staining to detect apoptosis induced by QM-DMAC in drug-resistant A549/DDP cells. As shown in Fig. 6E, approximately 79.6 % of A549/DDP cells undergo apoptosis following the combined therapy (CDDP + QM-DMAC + L). Collectively, these findings further demonstrate that, upon white light irradiation, QM-DMAC significantly enhances the chemotherapeutic effect by inducing ROS generation, triggering ROS-induced LMP, and accelerating apoptosis in drug-resistant tumor cells, indicating its considerable potential as an effective chemosensitizer.

Furthermore, we expanded our investigation to evaluate the *in vivo* chemosensitization efficacy of QM-DMAC in drug-resistant A549/DDP tumor. The tumor volumes in the QM-DMAC + L and combined therapy

(CDDP + QM-DMAC + L) groups were markedly reduced (Fig. 6F and G). Moreover, the anticancer activity of the CDDP + QM-DMAC + L group was particularly pronounced, indicating that QM-DMAC significantly enhances the anticancer effect of chemotherapy upon white light irradiation, particularly against drug-resistant tumors. These results undoubtedly reinforced the potential of QM-DMAC as an efficient chemosensitizer.

3. Conclusion

In summary, we have designed and synthesized a unique AIE-active luminogen, QM-DMAC, which possesses extraordinary bioimaging and therapeutic abilities. QM-DMAC shows typical AIE characteristics, and fluorescence response to viscosity changes. QM-DMAC can be effectively utilized for lysosome-specific imaging in live-cells, offering a high signal-to-noise ratio and displaying favorable biocompatibility. Leveraging its viscosity-responsive properties and lysosome-specific targeting capabilities, QM-DMAC is capable of specifically visualizing changes in lysosome viscosity under different conditions within living cells, including drug-induced inflammation and autophagy. This ability can provide valuable diagnostic information in clinical practice, helping clinicians to monitor disease progression at the cellular level and to make tumor treatment protocols more precisely. Additionally, it can effectively discriminate between tumor and normal cells, given that lysosomal viscosity is typically higher in tumor cells, helping early detection and intervention of tumors. Furthermore, QM-DMAC can generate a substantial amount of ROS in tumor cells upon white light irradiation, which precisely induces ROS-mediated LMP and subsequent lysosomal damage. This not only specifically boosts the efficacy of PDT but also re-sensitizes tumor cells to low-dose radiotherapy and chemotherapy, thereby dramatically enhancing the combined therapeutic antitumor effect. This multimodal therapeutic strategy can effectively address the limitations of monotherapy, such as insufficient sensitivity or the development of resistance at the cellular and subcellular levels, and can also significantly reduce the doses of conventional chemotherapeutic agents and radiation therapy required, thereby maximizing antitumor efficacy while reducing side effects. Ultimately, it has been demonstrated that the AIE PS QM-DMAC can efficiently hijack tumor lysosomes, acting as an excellent therapeutic sensitizer and exhibiting extraordinarily impressive antitumor efficiency, even against drug-resistant tumors. This study is expected to offer a powerful theranostic platform for overcoming clinical therapeutic resistance and to provide insights into the design of a new generation of cancer theranostics for potential clinical applications.

CRediT authorship contribution statement

Hang Zou: Writing – original draft, Methodology, Funding acquisition, Formal analysis, Data curation. **Pingping Wang:** Methodology, Data curation. **Zhihao Bai:** Writing – review & editing, Methodology, Data curation. **Liping Liu:** Investigation, Data curation. **Jingtong Wang:** Methodology, Data curation. **Yanfang Cheng:** Methodology, Formal analysis. **Bairong He:** Writing – review & editing, Methodology, Data curation. **Zujin Zhao:** Writing – review & editing, Visualization, Investigation. **Lei Zheng:** Validation, Supervision, Resources, Investigation, Funding acquisition.

Declaration of competing interest

The authors declare that they have no known competing financial interests or personal relationships that could have appeared to influence the work reported in this paper.

Acknowledgements

H. Zou, P. P. Wang and Z. H. Bai contributed equally to this work.

This work was financially supported by the National Natural Science Foundation of China (82302647), the National Science Fund for Distinguished Young Scholars (82025024), the Outstanding Youths Development Scheme of Nanfang Hospital, Southern Medical University (2023J007), the Science and Technology Projects in Guangzhou (2024A04J5115), and the President Foundation of Nanfang Hospital, Southern Medical University (2021C047, 2021C042).

Appendix A. Supplementary data

Supplementary data to this article can be found online at https://doi.org/10.1016/j.mtbio.2025.101564.

Data availability

Supplementary data to this article can be found online

References

[1] X. Shi, X. Wang, W. Yao, D. Shi, X. Shao, Z. Lu, Y. Chai, J. Song, W. Tang, X. Wang, Mechanism insights and therapeutic intervention of tumor metastasis: latest developments and perspectives, Signal Transduct. Targeted Ther. 9 (1) (2024) 192, https://doi.org/10.1038/s41392-024-01885-2.

[2] H. Liu, X. Chen, Y. Jia, H. Chen, X. Wang, G. Liu, Y. Luo, Facing inevitable PARPis resistance: mechanisms and therapeutic strategies for breast cancer treatment, Interdiscip. Med. 1 (2) (2023) e20220013, https://doi.org/10.1002/INMD.20220013.

[3] Y. Pu, L. Li, H. Peng, L. Liu, D. Heymann, C. Robert, F. Vallette, S. Shen, Drug-tolerant persister cells in cancer: the cutting edges and future directions, Nat. Rev. Clin. Oncol. 20 (11) (2023) 799–813, https://doi.org/10.1038/s41571-023-00815-5.

[4] F. Weiss, D. Lauffenburger, P. Friedl, Towards targeting of shared mechanisms of cancer metastasis and therapy resistance, Nat. Rev. Cancer 22 (3) (2022) 157–173, https://doi.org/10.1038/s41568-021-00427-0.

[5] A. Marusyk, M. Janiszewska, K. Polyak, Intratumor heterogeneity: the Rosetta stone of therapy resistance, Cancer Cell 37 (4) (2020) 471–484, https://doi.org/10.1016/j.ccell.2020.03.007.

[6] J. Liu, J. Wu, T. Chen, B. Yang, X. Liu, J. Xi, Z. Zhang, Y. Gao, Z. Li, Enhancing X-ray sensitization with multifunctional nanoparticles, Small 20 (35) (2024) 2400954, https://doi.org/10.1002/smll.202400954.

[7] Q. Fu, C. Wei, X. Yang, M. Wang, J. Song, Biomarker-induced gold aggregates enable activatable near-infrared-II photoacoustic image-guided radiosensitization, Aggregate (2024) e652, https://doi.org/10.1002/agt2.652.

[8] E. Khatoon, K. Banik, C. Harsha, B.L. Sailo, K.K. Thakur, A.D. Khwairakpam, R. Vikkurthi, T.B. Devi, S.C. Gupta, A.B. Kunnumakkara, Phytochemicals in cancer cell chemosensitization: current knowledge and future perspectives, Semin. Cancer Biol. 80 (2022) 306–339, https://doi.org/10.1016/j.semcancer.2020.06.014.

[9] C. Cheng, W. Jiang, Y. Luo, L. Wan, X. Guo, Z. Xie, R. Tang, T. Huang, J. Wang, C. Du, Z. Wang, H. Ran, P. Li, Z. Zhou, J. Ren, NIR activated multimodal therapeutics based on metal-phenolic networks-functionalized nanoplatform for combating against multidrug resistance and metastasis, Small 19 (14) (2023) 2206174, https://doi.org/10.1002/smll.202206174.

[10] L.K. Mell, S.J. Wong, Good radiosensitizer hunting, J. Clin. Oncol. 41 (13) (2023) 2313–2318, https://doi.org/10.1200/JCO.22.02350.

[11] A. Ballabio, J.S. Bonifacino, Lysosomes as dynamic regulators of cell and organismal homeostasis, Nat. Rev. Mol. Cell Biol. 21 (2) (2020) 101–118, https://doi.org/10.1038/s41580-019-0185-4.

[12] B. Banushi, S.R. Joseph, B. Lum, J.J. Lee, F. Simpson, Endocytosis in cancer and cancer therapy, Nat. Rev. Cancer 23 (7) (2023) 450–473, https://doi.org/10.1038/s41568-023-00574-6.

[13] J. Liu, L. Ren, S. Li, W. Li, X. Zheng, Y. Yang, W. Fu, J. Yi, J. Wang, G. Du, The biology, function, and applications of exosomes in cancer, Acta Pharm. Sin. B 11 (9) (2021) 2783–2797, https://doi.org/10.1016/j.apsb.2021.01.001.

[14] N.A. Hussein, S. Malla, M.A. Pasternak, D. Terrero, N.G. Brown, C.R. Ashby Jr., Y. G. Assaraf, Z.S. Chen, A.K. Tiwari, The role of endolysosomal trafficking in anticancer drug resistance, Drug Resist. Updates 57 (2021) 100769, https://doi.org/10.1016/j.drup.2021.100769.

[15] B. Zhitomirsky, Y.G. Assaraf, Lysosomes as mediators of drug resistance in cancer, Drug Resist. Updates 24 (2016) 23–33, https://doi.org/10.1016/j.drup.2015.11.004.

[16] H. Meyer, B. Kravic, The endo-lysosomal damage response, Annu. Rev. Biochem. 93 (1) (2024) 367–387, https://doi.org/10.1146/annurev-biochem-030222-102505.

[17] Y. He, Y. Fan, X. Ahmadpoor, Y. Wang, Z.A. Li, W. Zhu, H. Lin, Targeting lysosomal quality control as a therapeutic strategy against aging and diseases, Med. Res. Rev. 44 (6) (2024) 2472–2509, https://doi.org/10.1002/med.22047.

[18] P. Pihan, F. Lisbona, J. Borgonovo, S. Edwards-Jorquera, P. Nunes-Hasler, K. Castillo, O. Kepp, H. Urra, S. Saarnio, H. Vihinen, A. Carreras-Sureda, S. Forveille, A. Sauvat, D. De Giorgis, A. Pupo, D.A. Rodriguez, G. Quarato, A. Sagredo, F. Lourido, A. Letai, R. Latorre, G. Kroemer, N. Demaurex, E. Jokitalo,

M.L. Concha, A. Glavic, D.R. Green, C. Hetz, Control of lysosomal-mediated cell death by the pH-dependent calcium channel RECS1, Sci. Adv. 7 (46) (2021), https://doi.org/10.1126/sciadv.abe5469 eabe5469.
[19] X. Yuan, W. Nie, Z. He, J. Yang, B. Shao, X. Ma, X. Zhang, Z. Bi, L. Sun, X. Liang, Y. Tie, Y. Liu, F. Mo, D. Xie, Y. Wei, X. Wei, Carbon black nanoparticles induce cell necrosis through lysosomal membrane permeabilization and cause subsequent inflammatory response, Theranostics 10 (10) (2020) 4589–4605, https://doi.org/10.7150/thno.34065.
[20] M.A. Lucherelli, X. Qian, P. Weston, M. Eredia, W. Zhu, P. Samori, H. Gao, A. Bianco, A. von dem Bussche, Boron nitride nanosheets can induce water channels across lipid bilayers leading to lysosomal permeabilization, Adv. Mater. 33 (45) (2021) e2103137, https://doi.org/10.1002/adma.202103137.
[21] B. Jana, S. Jin, E.M. Go, Y. Cho, D. Kim, S. Kim, S.K. Kwak, J.H. Ryu, Intra-lysosomal peptide assembly for the high selectivity index against cancer, J. Am. Chem. Soc. 145 (33) (2023) 18414–18431, https://doi.org/10.1021/jacs.3c04467.
[22] M. Cao, X. Luo, K. Wu, X. He, Targeting lysosomes in human disease: from basic research to clinical applications, Signal Transduct. Targeted Ther. 6 (1) (2021) 379, https://doi.org/10.1038/s41392-021-00778-y.
[23] T.C. Pham, V.N. Nguyen, Y. Choi, S. Lee, J. Yoon, Recent strategies to develop innovative photosensitizers for enhanced photodynamic therapy, Chem. Rev. 121 (21) (2021) 13454–13619, https://doi.org/10.1021/acs.chemrev.1c00381.
[24] Z. Liu, H. Zou, Z. Zhao, P. Zhang, G.G. Shan, R.T.K. Kwok, J.W.Y. Lam, L. Zheng, B. Z. Tang, Tuning organelle specificity and photodynamic therapy efficiency by molecular function design, ACS Nano 13 (10) (2019) 11283–11293, https://doi.org/10.1021/acsnano.9b04430.
[25] J. Choi, I.C. Sun, H. Sook Hwang, H. Yeol Yoon, K. Kim, Light-triggered photodynamic nanomedicines for overcoming localized therapeutic efficacy in cancer treatment, Adv. Drug Deliv. Rev. 186 (2022) 114344, https://doi.org/10.1016/j.addr.2022.114344.
[26] Y. Zhang, Y. Wan, Y. Chen, N.T. Blum, J. Lin, P. Huang, Ultrasound-enhanced chemo-photodynamic combination therapy by using albumin "Nanoglue"-Based nanotheranostics, ACS Nano 14 (5) (2020) 5560–5569, https://doi.org/10.1021/acsnano.9b09827.
[27] M. Pan, Q. Jiang, J. Sun, Z. Xu, Y. Zhou, L. Zhang, X. Liu, Programming DNA nanoassembly for enhanced photodynamic therapy, Angew. Chem. Int. Ed. 59 (5) (2020) 1897–1905, https://doi.org/10.1002/anie.201912574.
[28] Y.H. Li, H.R. Jia, H.Y. Wang, X.W. Hua, Y.W. Bao, F.G. Wu, Mitochondrion, lysosome, and endoplasmic reticulum: which is the best target for phototherapy? J. Contr. Release 351 (2022) 692–702, https://doi.org/10.1016/j.jconrel.2022.09.037.
[29] M. Yang, Z. Zeng, J.W.Y. Lam, J. Fan, K. Pu, B.Z. Tang, State-of-the-art self-luminescence: a win-win situation, Chem. Soc. Rev. 51 (21) (2022) 8815–8831, https://doi.org/10.1039/d2cs00228k.
[30] B. Yu, M. Liu, L. Jiang, C. Xu, H. Hu, T. Huang, D. Xu, N. Wang, Q. Li, B.Z. Tang, X. Huang, W. Zhang, Aggregation-induced emission photosensitizer-engineered anticancer nanomedicine for synergistic chemo/chemodynamic/photodynamic therapy, Adv. Healthcare Mater. 13 (11) (2024) 2303643, https://doi.org/10.1002/adhm.202303643.
[31] Y. Liao, Z. Peng, X. Liu, Y. Hu, J. Zhang, Theranostic applications of biomolecule-responsive aggregation-induced emission luminogens, Interdiscip. Med. 1 (4) (2023) e20230024, https://doi.org/10.1002/INMD.20230024.
[32] X. Cai, B. Liu, Aggregation-induced emission: recent advances in materials and biomedical applications, Angew. Chem. Int. Ed. 59 (25) (2020) 9868–9886, https://doi.org/10.1002/anie.202000845.
[33] B. Wu, Kenry, F. Hu, Targeted antibacterial photodynamic therapy with aggregation-induced emission photosensitizers, Interdiscip. Med. 2 (1) (2024) e20230038, https://doi.org/10.1002/INMD.20230038.
[34] Z. Zheng, Y. Yang, P. Wang, X. Gou, J. Gong, X. Wu, Z. Bao, L. Liu, J. Zhang, H. Zou, L. Zheng, B.Z. Tang, A bright two-photon lipid droplets probe with viscosity-enhanced solvatochromic emission for visualizing lipid metabolic disorders in Deep tissues, Adv. Funct. Mater. 33 (35) (2023) 2303627, https://doi.org/10.1002/adfm.202303627.
[35] Z. Zhuang, J. Li, P. Shen, Z. Zhao, B.Z. Tang, Exploring and leveraging aggregation effects on reactive oxygen species generation in photodynamic therapy, Aggregate 5 (4) (2024) e540, https://doi.org/10.1002/agt2.540.
[36] J. Jia, Z. Ma, J. Zhuang, L. Huo, C. Zhou, N. Li, N. Zhao, Lipid droplet-targeted NIR AIE photosensitizer evoking concurrent ferroptosis and apoptosis, Aggregate 5 (3) (2024) e516, https://doi.org/10.1002/agt2.516.
[37] Y. Wang, J. Liao, Y. Lyu, Q. Guo, Z. Zhu, X. Wu, J. Yu, Q. Wang, W.-H. Zhu, An AIE photosensitizer with simultaneous type I and type II ROS generation: efficient bacterial elimination and hypoxic tumor ablation, Adv. Funct. Mater. 33 (33) (2023) 2301692, https://doi.org/10.1002/adfm.202301692.
[38] Z. Guo, C. Yan, W.-H. Zhu, High-performance quinoline-malononitrile core as a building block for the diversity-oriented synthesis of AIEgens, Angew. Chem. Int. Ed. 59 (25) (2020) 9812–9825, https://doi.org/10.1002/anie.201913249.
[39] X. Wu, J. Zeng, X. Peng, H. Liu, B.Z. Tang, Z. Zhao, Robust sky-blue aggregation-induced delayed fluorescence materials for high-performance top-emitting OLEDs and single emissive layer white OLEDs, Chem. Eng. J. 451 (2023) 138919, https://doi.org/10.1016/j.cej.2022.138919.
[40] S. Xu, Y. Yuan, X. Cai, C.-J. Zhang, F. Hu, J. Liang, G. Zhang, D. Zhang, B. Liu, Tuning the singlet-triplet energy gap: a unique approach to efficient photosensitizers with aggregation-induced emission (AIE) characteristics, Chem. Sci. 6 (10) (2015) 5824–5830, https://doi.org/10.1039/C5SC01733E.
[41] J. Mei, Y. Hong, J.W.Y. Lam, A. Qin, Y. Tang, B.Z. Tang, Aggregation-induced emission: the whole is more brilliant than the parts, Adv. Mater. 26 (31) (2014) 5429–5479, https://doi.org/10.1002/adma.201401356.
[42] Y. Hong, J.W.Y. Lam, B.Z. Tang, Aggregation-induced emission: phenomenon, mechanism and applications, Chem. Commun. (29) (2009) 4332–4353, https://doi.org/10.1039/B904665H.
[43] Z. Zhuang, J. Dai, M. Yu, J. Li, P. Shen, R. Hu, X. Lou, Z. Zhao, B.Z. Tang, Type I photosensitizers based on phosphindole oxide for photodynamic therapy: apoptosis and autophagy induced by endoplasmic reticulum stress, Chem. Sci. 11 (13) (2020) 3405–3417, https://doi.org/10.1039/d0sc00785d.
[44] X.Y. Ran, W.L. Xia, L.N. Zhang, X.Q. Yu, P. Chen, K.P. Xie, Y. Zhao, C. Yi, K. Li, *De novo* design of type-l photosensitizer agents based on structure-inherent low triplet energy for hypoxia photodynamic therapy, Mater. Horiz. 11 (22) (2024) 5589–5599, https://doi.org/10.1039/d4mh01167h.
[45] J. Yin, L. Huang, L. Wu, J. Li, T.D. James, W. Lin, Small molecule based fluorescent chemosensors for imaging the microenvironment within specific cellular regions, Chem. Soc. Rev. 50 (21) (2021) 12098–12150, https://doi.org/10.1039/d1cs00645b.
[46] J. Guo, L. Fan, Q. Zan, J. Wang, Z. Yang, W. Lu, Y. Yang, X. Yang, C. Dong, S. Shuang, Rational design of orange-red emissive carbon dots for tracing lysosomal viscosity dynamics in living cells and zebrafish, Anal. Chem. 95 (32) (2023) 12139–12151, https://doi.org/10.1021/acs.analchem.3c02381.
[47] R. Nanayakkara, R. Gurung, S.J. Rodgers, M.J. Eramo, G. Ramm, C.A. Mitchell, M. J. McGrath, Autophagic lysosome reformation in health and disease, Autophagy 19 (5) (2023) 1378–1395, https://doi.org/10.1080/15548627.2022.2128019.
[48] Y. Lyu, X. Chen, Q. Wang, Q. Li, Q. Wang, X. Li, Z. Zhu, C. Yan, X. Zhao, W.-H. Zhu, Monitoring autophagy with Atg4B protease-activated aggregation-induced emission probe, Adv. Funct. Mater. 32 (6) (2022) 2108571, https://doi.org/10.1002/adfm.202108571.
[49] Y. Song, H. Zhang, X. Wang, X. Geng, Y. Sun, J. Liu, Z. Li, One stone, three birds: pH triggered transformation of aminopyronine and iminopyronine based lysosome targeting viscosity probe for cancer visualization, Anal. Chem. 93 (3) (2021) 1786–1791, https://doi.org/10.1021/acs.analchem.0c04644.
[50] Y. Yao, R. Xu, W. Shao, J. Tan, S. Wang, S. Chen, A. Zhuang, X. Liu, R. Jia, A novel nanozyme to enhance radiotherapy effects by lactic acid scavenging, ROS generation, and hypoxia mitigation, Adv. Sci. 11 (26) (2024) 2403107, https://doi.org/10.1002/advs.202403107.
[51] L.L. Zhou, Q. Guan, W. Zhou, J.L. Kan, K. Teng, M. Hu, Y.B. Dong, A multifunctional covalent organic framework nanozyme for promoting ferroptotic radiotherapy against esophageal cancer, ACS Nano 17 (20) (2023) 20445–20461, https://doi.org/10.1021/acsnano.3c06967.
[52] S.R. Bonam, F. Wang, S. Muller, Lysosomes as a therapeutic target, Nat. Rev. Drug Discov. 18 (12) (2019) 923–948, https://doi.org/10.1038/s41573-019-0036-1.
[53] Y. Han, P. Wen, J. Li, K. Kataoka, Targeted nanomedicine in cisplatin-based cancer therapeutics, J. Contr. Release 345 (2022) 709–720, https://doi.org/10.1016/j.jconrel.2022.03.049.
[54] W. Jiang, Z. Tie, C. Yu, Y. Chen, D. Liu, B. Li, An engineered nanoplatform inhibiting energy metabolism and lysosomal activity of tumor cells to multiply cisplatin-based chemotherapy, Biomaterials 302 (2023) 122354, https://doi.org/10.1016/j.biomaterials.2023.122354.